Journal of Hazardous Materials 174 (2010) 129–136

Contents lists available at ScienceDirect

Journal of Hazardous Materials

journal homepage: www.elsevier.com/locate/jhazmat

Si-doped mesoporous TiO_2 continuous fibers: Preparation by centrifugal spinning and photocatalytic properties

Nan Bao*, Zhentao Wei, Zhihui Ma, Feng Liu, Guangbin Yin

School of Environmental Science and Engineering, Shandong University, Ji'nan 250100, PR China

ARTICLE INFO

Article history:
Received 5 March 2009
Received in revised form 9 July 2009
Accepted 7 September 2009
Available online 12 September 2009

Keywords:
Titania
Centrifugal spinning
Si-doped
Mesoporous
Continuous fiber

ABSTRACT

TiO_2 continuous fibers were prepared by a sol–gel method combined with centrifugal spinning without any template or binder polymer. The fibers were characterized using XRD, FT-IR, SEM, N_2 adsorption–desorption, and UV–vis DRS. The addition of silica was a crucial factor for obtaining long fibers because of the formation of Ti–O–Si networks. The effects of dopant contents and heat treatment temperatures were studied. It was found that the proper addition of silica into titania could improve the surface texture and enhance the thermal stability and crystal stability. When Si/Ti molar ratio was 0.15, mesoporous TiO_2 fibers with a BET surface area up to 127.7 $m^2\ g^{-1}$ were obtained after heat treatment at 700 °C. It displayed the highest photoactivity of all, and the degradation rate of X-3B in aqueous solution reached 99.6% after 75 min under UV irradiation. Furthermore, the degradation rate and the mineralization rate of X-3B were 94.7% and 58.9% after 3 h under solar irradiation, respectively. In addition, it was worthwhile to mention that the degradation efficiency was also more than 90% after 6 cycles.

1. Introduction

Advanced oxidation processes (AOPs) based on UV-radiation and TiO_2 are promising technologies for the removal of organic contaminates from water attributed to the generation of highly reactive radical species such as $^{\bullet}OH$ and $^{\bullet}O_2^-$. It is generally accepted that anatase is the most active of the three phases of TiO_2 (anatase, rutile and brookite) [1,2]. But the recombination ratio of photo-induced electrons (e^-) and positive holes (h^+) produced from the interior of pure TiO_2 under the irradiation of UV light ($\lambda < 380$ nm) is so high that the photocatalytic efficiency of TiO_2 by degrading pollutants is decreased greatly. In recent years, more and more attention has been put on the modification of titanium dioxide for improving the photoactivity of TiO_2, such as the noble metal deposition on the surface, the adulteration of transition metals, the surface photosensitization and the combination of two different semiconductors [3].

Much work has been conducted on preparing nanopowders of TiO_2 which have excellent photocatalytic activity [4,5]. In addition, various new morphology such as nanorods, nanoflowers [6], nanotubes [7], nanofibers [8] and hollow spheres [9,10] have been prepared. But application of these materials, especially in water purification, is still facing challenge due to difficult separation from solution because of their microsize [11]. At the same time, the technology of mounting the TiO_2 on supports for recycling [12] also has some shortcomings. Therefore, self-supporting TiO_2 fibers have been the subject of intensive research as late-model photocatalysts. Although fibrous TiO_2-based materials have been prepared by sol–gel reaction [13,14], solvothermal reaction [15–18], and ion-exchange reaction [19], the lengths are only several millimeters or centimeters and the BET surface area is also extremely low.

Long continuous TiO_2 fibers have revealed enormous advantages in water treatment, and some researchers have synthesized them by a sol–gel process. Generally, the templates are absolutely necessary for obtaining precursor fibers. After subsequent calcination, the templates are removed, and ordered periodic structures are formed. Madhugiri et al. [20] successfully prepared mesoporous TiO_2 fibers using Pluronic 123 as template. But heating the fibers further to 600 °C sharply reduced the surface area to 32 $m^2\ g^{-1}$, and the photocatalytic properties fell well below those of commercial catalysts. Zhan et al. [21] also prepared long TiO_2 hollow fibers with mesoporous walls using Pluronic 123 as template, which exhibited high photocatalytic activity. However, the thermal stability was not satisfying. It was found that the rutile phase formed and mesopores disappeared as a result of the collapse of the pore structure at 800 °C. In addition, the cost of template-additives was increased. Ishikawa et al. [22] treated a polycarbosilane (PCS) with $Ti(OC_4H_9)_4$, and created a strong, fibrous photocatalyst with a surface TiO_2 layer by melt spinning. Their new technology made full use of the bleed-out phenomenon of additives intentionally mixed in the PCS. But the BET surface area of this material was only 11 $m^2\ g^{-1}$ after the HF etching for 75 min, and parts of TiO_2 layer were dropped from

* Corresponding author. Tel.: +86 13645418916; fax: +86 53188364513.
E-mail address: baonan@sdu.edu.cn (N. Bao).

0304-3894/$ – see front matter © 2009 Elsevier B.V. All rights reserved.
doi:10.1016/j.jhazmat.2009.09.026

the silica core structure for more than 90 min [23]. Consequently, it is necessary to find new economical preparation processes to get benign photocatalysts.

In this paper, long mesoporous nano-TiO_2 fibers containing different silica contents were synthesized without any template by a sol–gel method followed centrifugal spinning. We could control the crystal phase, surface area and porous structure by varying the contents of silica and the heat treatment temperatures in steam. Photocatalytic activity of the fibers had been tested in terms of degradation of reactive brilliant red X-3B. According to the results, we discussed the effects of silica addition and heat treatment temperatures for the photoactivity.

2. Experimental

2.1. Chemicals and materials

Titanium tetrabutoxide (TBOT), tetraethyl orthosilicalite (TEOS), isopropyl alcohol (IPA), ethyl acetoacetate (EAcAc) and tetrahydrofuran (THF) were purchased from Sinopharm International Company Ltd. (Shanghai, China). Reactive brilliant red X-3B was purchased from Shanghai Dyestuff Chemical Plant, whose structure is shown as Fig. 1. All the chemical reagents were of analytical grade and used without further purification. Deionized water was used in all experiments.

2.2. Preparation of catalyst

TBOT and TEOS were used as sources of titanium and silicon, respectively. The molar ratio of TBOT:EAcAc:H_2O:TEOS in the study was 1:0.4:1.5:Y where Y depends on the Si/Ti molar ratio (0.05–0.20). First of all, TBOT was added to the EAcAc/IPA solution, refluxed in N_2 for 1 h. Then, a titania sol of TBOT:EAcAc:H_2O = 1:0.4:1.5 in EPA was produced by hydrolysis and condensation by dropwise addition of a H_2O/EPA solution with continuous refluxing in nitrogen atmosphere. After the reaction was completed, the sol was dried at 143 °C to obtain brownish yellow powders. Subsequently, the powders were dissolved in THF containing corresponding content of TEOS, followed by refluxing for 1 h. After centrifugation, stable titania–silica sol was obtained.

The sol was evaporated by a rotary evaporator to prepare the spinnable solution, corresponding to the viscosity of 2 Pa s. Then, long continuous precursor fibers were obtained by using the self-made centrifugal spinning apparatus (Fig. 2), which was highly efficient, robust and easy to operate [24]. First, the spinnable solution was injected into centrifugal tube inserted into rotational mold. And then it was thrown through a small hole (diameter: 0.5 mm) at a speed of 6500 rpm/min to produce fibers, which were collected by a cylindrical mesh. For high photoactivity, the as-prepared precursor fibers were placed in a tube furnace and heat-treated in steam atmosphere (3 mL min^{-1}) at different temperatures by stage-temperature-programmed technique, which could achieve step-heating. The finished fibers were designated as XSTF-T, where X is the Si/Ti molar ratio and T denotes the highest heat treatment temperature. For comparison, pure TiO_2 samples were synthesized by the same method just without TEOS and denoted PTF-T.

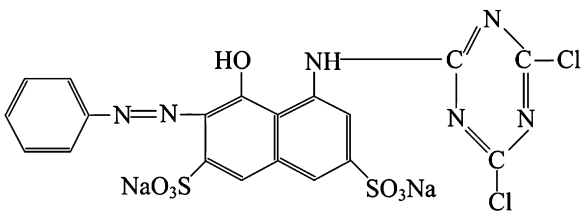

Fig. 1. Molecule structure of dye X-3B.

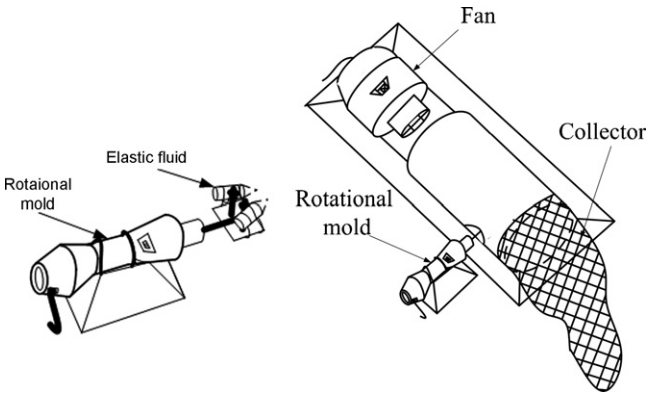

Fig. 2. Schematic illustration of the centrifugal spinning apparatus.

2.3. Characterization of prepared photocatalyst

The surface morphologies of the fibers were observed by scanning electron microscope (S-520, Hitachi, Japan). N_2 adsorption–desorption isotherms were obtained by using a Quadrasorb SI-MP system (Quantachrome, USA). All samples were degassed at 573 K for 8 h in vacuum before BET measurements. The Brunauer–Emmett–Teller (BET) specific surface area was determined by a multipoint BET method using the adsorption data in the relative pressure (p/p_0) range of 0.05–0.3. The pore size distribution was calculated using the DFT method. The N_2 adsorption volume at the relative pressure (p/p_0) of 0.991 was used to determine the pore volume and the average pore size. The crystal structure of TiO_2 fibers was analyzed with X-ray diffraction (D/max-γA, Rigaku, Japan), operated at 40 kV and 70 mA, using Cu K_α radiation (λ = 0.154178 nm) and at a scanning ratio of 10°/min in 2θ ranging from 20° to 70°. The particle diameter (D) was calculated by applying the Scherer's equation: $D = 0.89\lambda/(B\cos\theta)$, where λ is the X-ray wavelength, θ is the Bragg angle and B is the full width at half maxima. The mass fraction of the rutile phase (X_R) was calculated by the equation [25]: $X_R = 1/(1 + 0.8I_A/I_R)$, where I_A and I_R is the intensity of the reflections corresponding to the anatase (1 0 1) and rutile (1 1 0) structure, respectively. FT-IR spectra were recorded using an Avatar 370 spectrometer (Thermo Nicolet, USA). The zeta-potential of the PTF-700 and 0.15STF-700 was measured using a zeta-potential analyzer (DXD-II, China). Solid state UV–vis diffuse reflectance spectra were recorded at room temperature and in air by means of a UV–vis spectrophotometer (UV-3100, Shimadzu, Japan) equipped with an integrating sphere attachment using $BaSO_4$ as background.

2.4. Photoactivity studies

2.4.1. Laboratory experiments

All the experiments were performed in an open fixed-bed photo-reactor [26], fitted with a 250 W high-pressure mercury lamp (λ_{max} = 365 nm). The irradiation intensity (15 W m^{-2}) of the lamp at the surface of dye solution was measured with digital illuminometer (TN-2340, Taiwan). Before irradiation, the aqueous solution of X-3B (100 mL) with an initial concentration 20 mg L^{-1} in the presence of 0.4 g prepared TiO_2 fibers was stirred circularly for 30 min under darkness. Then, the reaction mixture was illuminated with the high-pressure mercury lamp, and cycled by a peristaltic pump (flow rate 20 mL min^{-1}) for the entire time span of experiment. At regular intervals, samples of about 5 mL in volume were taken and filtrated in a 0.45 μm syringe filter. The supernates were analyzed by recording the variations of the maximum

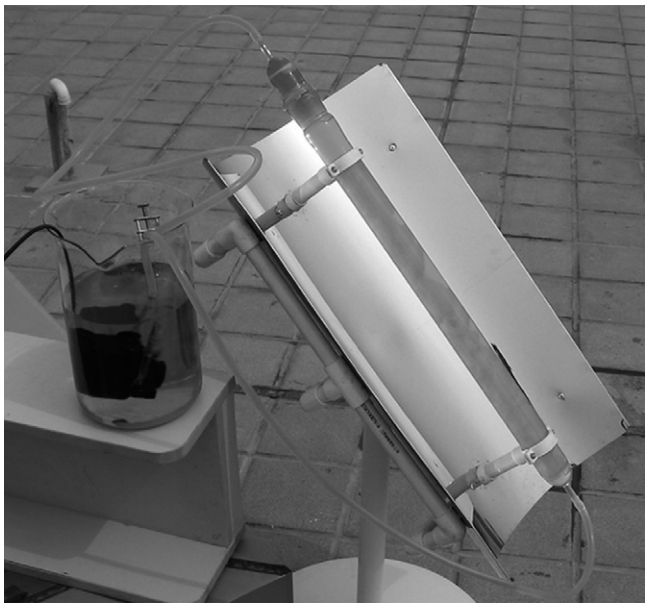

Fig. 3. Experimental apparatus for solar pohotocatalytic reaction.

absorption wave-length (536 nm) using a UV–vis 1601 spectrophotometer (Shimadzu, Japan). The determined absorbance was converted to concentration through the standard curve method of X-3B. The degradation efficiency of X-3B was calculated by $R = (1 - C/C_0) \times 100\%$, where C_0 and C were the concentration of X-3B when reaction time was 0 and t, respectively.

2.4.2. Solar experiments

The solar experiment was carried out in a self-made photoreactor shown in Fig. 3, which was composed of three parts: a quartz-tube (length: 50 cm, diameter: 4 cm) as the reaction vessel, a concave aluminous board, and a fixed rack of a 37° dip angle. Direct sunlight was used in this study and the experiment was conducted between 11:30 a.m. and 2:30 p.m. when the solar intensity fluctuations were minimal. The average solar intensity was 0.724 kW m^{-2} (5 June 2008, Jinan) with the radiometer (TES-1339, Taiwan). In the experimental process, 5 g TiO_2 fibers were placed in the quartz-tube packed with porous plates on both ends to prevent outflow of fibers. 20 mg L^{-1} aqueous solution of X-3B (3 L) was pumped through the reaction tube (flow rate 2 L h^{-1}) to achieve continuous degradation. After 3 h, the degradation rate of X-3B was calculated according to the above method. In addition, mineralization rate of X-3B was obtained by total organic carbon analyzer (TOC-5000A, Shimadzu, Japan).

3. Results and discussion

3.1. XRD measurements

XRD was used to characterize the phase structure of the as-prepared samples. The XRD patterns of PTF and 0.15STF prepared at different temperatures were shown in Fig. 4. It can be observed that there was no significant change in the diffraction peaks at corresponding diffraction angles of anatase phase (JCPDS no. 21-1272) in the pure titania samples heated at temperatures below 600 °C. As the heat-treated temperature was increased up to 700 °C, the rutile (JCPDS no. 21-1276) appeared in pure titania sample, indicating that PTF-700 was the mixture of anatase and rutile phase with the ratio of anatase:rutile = 68:32 (Fig. 4(a)), whereas fully anatase phase was obtained at all temperatures by the addition of 0.15 molar ratio of silica (Fig. 4(b)). The samples of 0.15STF were

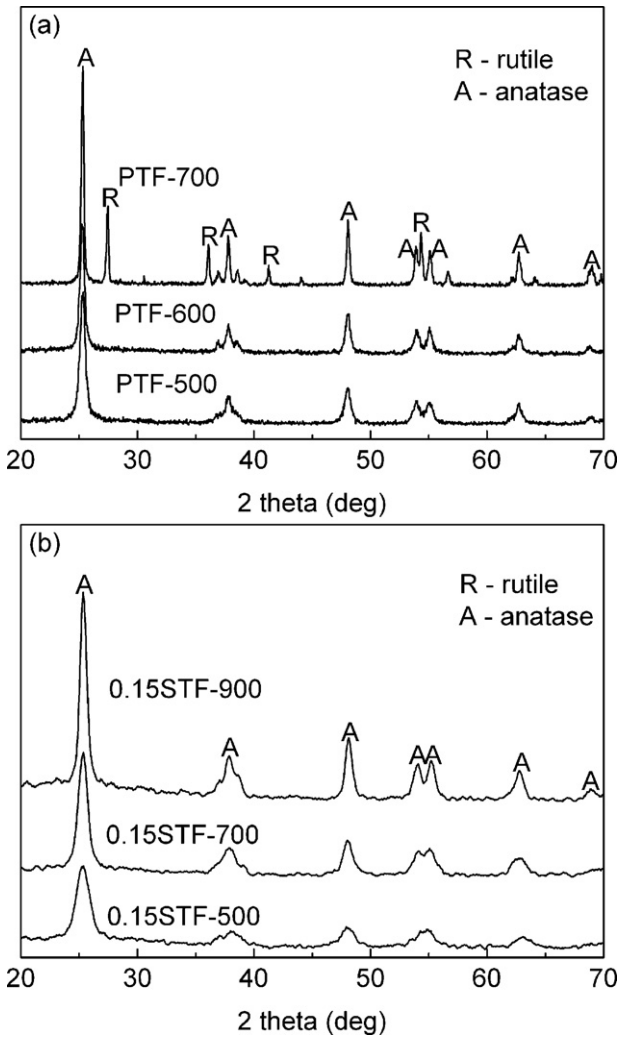

Fig. 4. XRD patterns of (a) PTF and (b) 0.15STF at different heat treatment temperatures.

detected as having a single-phase structure, and no trace of diffraction peaks due to other phases like silica or silicate was detected. This indicated that the proper amount of silica might be dissolved in titania matrix [27] and suppress the phase transformation of titania from anatase to rutile. Yoshinaka et al. [28] had reported the formation of an anatase solid solution containing up to ≈15 mol% SiO_2, which would be responsible for the observed inhibiting effect on the transformation of titania from anatase to rutile. The XRD spectra (figure is omitted) of all the Si-doped samples except 0.15STF heated at 700 °C also showed complete anatase phase.

Obviously, with increasing heat-treated temperatures, the peak intensity of anatase phase increased, while the width of the diffraction peak of anatase became narrower, indicating enhancement of crystallization and formation of larger crystallites. According to the result from the Scherrer's equation, the crystallite size of PTF sharply increased from 14.5 nm (500 °C) to 31.3 nm (700 °C). But the crystallite size of 0.15STF heat-treated at different temperatures 500, 700 and 900 °C was only 6.0, 8.5, and 11.9 nm, respectively. It was confirmed that the presence of silica could effectively prevent the growth of anatase crystal. The ionic radius of Si^{4+} (0.042 nm) is less than that of Ti^{4+} (0.068 nm) [27,29], this allows the movement of Si^{4+} ion into the titania matrix. The anatase solid solution with silica had high thermal stability, which resulted in suppression of phase transformation of titania from anatase to rutile. On the other hand, this substitution in the matrix would lead to the reduction

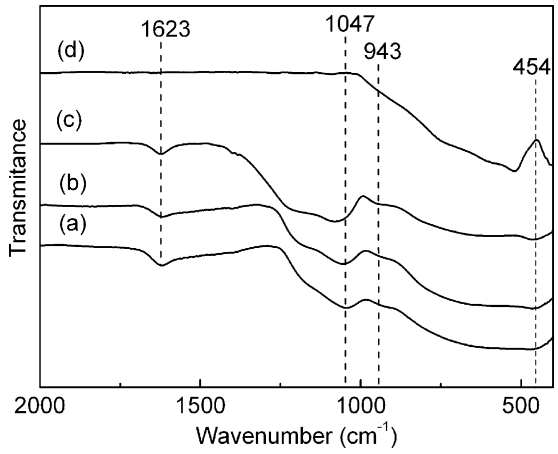

Fig. 5. Infrared spectra of (a) 0.15STF-500, (b) 0.15STF-700, (c) 0.15STF-900 and (d) PTF-700.

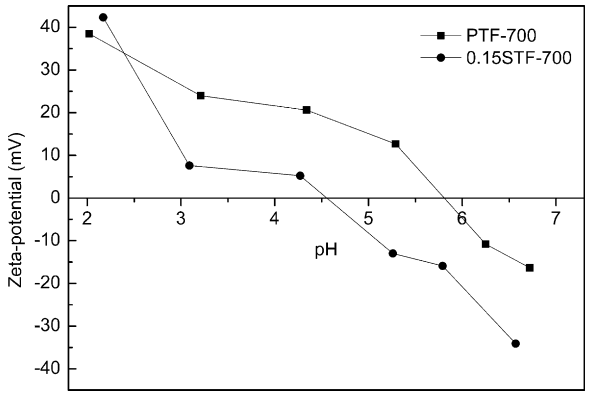

Fig. 6. Plot of the zeta-potential as a function of pH for the PTF-700 and 0.15STF-700 in the presence of $NaNO_3$ (10^{-3} M).

in anatase/anatase contact points which may reduce the growth of anatase crystal.

3.2. FT-IR spectroscopy

The IR spectra of TiO_2 samples with different composition at high temperatures were shown in Fig. 5. The band at 1047 cm^{-1} was attributed to the asymmetric stretching vibrations of Si–O–Si bond [30]. With the temperature increasing, the intensity of the Si–O–Si peak increased. It reflected that tetrahedral Si–O network structures were enhanced due to the hydrolysis and polycondensation of TEOS in steam atmosphere. The weak peak at 943 cm^{-1} was assigned to the asymmetric stretching vibration of Ti–O–Si [31], which evidenced the interaction between titania and silica at molecular-scale that can evidently enhance the surface properties and photocatalytic activity [32]. And the degree of dispersion at atomic level was commonly associated with the relative number of Ti–O–Si linkages [33]. In the work, the intensity of the Ti–O–Si peak increased slightly with increasing temperatures for 0.15STF. It indicated that higher temperature would be helpful for improving the homogeneity of mixed oxides because amorphous silica was dispersed in TiO_2 in a form of Si–O–Ti–O–Si networks [34] which were associated with the generation of Brønsted acidity [35,36]. The intensity of the band at 454 cm^{-1} attributed to the Ti–O–Ti stretching vibration of anatase phase [37], increased with increasing temperatures because of more perfect crystallization in agreement with the XRD results in which the peak became sharper and higher. The peak at 527 cm^{-1}, which only appeared in the spectra of PTF-700, could be assigned to the Ti–O–Ti stretching vibration of rutile phase [38]. Furthermore, the 1623 cm^{-1} band assigned to the surface hydroxyl groups was obviously observed except the sample of PTF-700. It could be also observed that there was no significant change in the intensity at 1623 cm^{-1} for the 0.15STF samples heat-treated at different temperatures from 500 to 900 °C. It was confirmed that an optimum amount of silica was beneficial for obtaining more surface hydroxyl groups and retaining them at the higher heat-treated temperature, which was helpful for improving photocatalytic activity. According to the above results, the Ti–O–Si bond and surface hydroxyl groups on the Ti–O network could suppress the nucleation of rutile TiO_2 and raise the phase transition temperature, which was coincided with the XRD results.

3.3. Zeta-potential of the catalyst

Fig. 6 showed the electrophoretic mobility data at different values of pH for the suspensions of PTF-700 and 0.15STF-700. The isoelectric point of 0.15STF-700 was 4.6 pH units, which was lower than 5.8 pH units for that of PTF-700, resulting in the equilibrium in Eq. (1) shifting to the left.

$$TiOH_2^+ \rightleftharpoons TiOH + H^+ \quad (1)$$

$$TiOH \rightleftharpoons TiO^- + H^+ \quad (2)$$

The presence of surface acidic groups resulting in the lower isoelectric point of TiO_2 had been reported [39,40]. The result implied that there were many acidic groups on the surface of 0.15STF-700. This might be because TiO_2–SiO_2 mixed oxides not only possessed Lewis acidity but also generated new Brønsted acid site, which was created when titania and silica formed Ti–O–Si chemical bonds [33]. Liu et al. [32] reported that the Brønsted acidity in atomically mixed TiO_2–SiO_2 oxides was correlated with the non-tetrahedral sites. In addition, surface hydroxylation was crucial to the presence of Brønsted acidity. Linsebigler et al. [41] had reported that hydroxyl groups on TiO_2 surface would accept holes generated by illumination and produce hydroxyl radicals which were strong oxidizing agents. Therefore, the sample of 0.15STF-700 had the potential to improving the photocatalytic activity because of the super hydrophilic nature of titania by inducing the Lewis acid sites in titania and the formation of •OH by surface –OH under UV irradiation.

3.4. SEM analysis

The SEM images of PTF-700 and 0.15STF-700 were shown in Fig. 7. From Fig. 7a, the PTF-700 was rough and collapsed with the diameters about 50 μm, and the length had only several millimeters. By comparison, the morphology of 0.15-Si/Ti precursor fibers were preserved after heat treatment at 700 °C, and the surface of the 0.15STF-700 was smooth with uniform diameters about 10–20 μm and average length about 1.1 m as shown in Fig. 7b. The formation of long Si-doped TiO_2 precursor fibers could be attributed to the addition of TEOS which favored a uniform sol through bonding interactions. In the subsequent heat treatment process, the amorphous silica and Ti–O–Si bonds prevented the fibers precursor from collapse and fracture [29]. Fig. 7c and d showed the observations of the surface of PTF-700 and 0.15STF-700, respectively. It could be seen that 0.15STF-700 was composed of nanoparticles and abundant pores, but the PTF-700 was nonporous. SEM analyses indicated that the formation of pores due to the removal of organics did not affect the overall image because of silica doping. Thus, heat treatment could result in large surface area and pore volume for Si-doped titania photocatalyst.

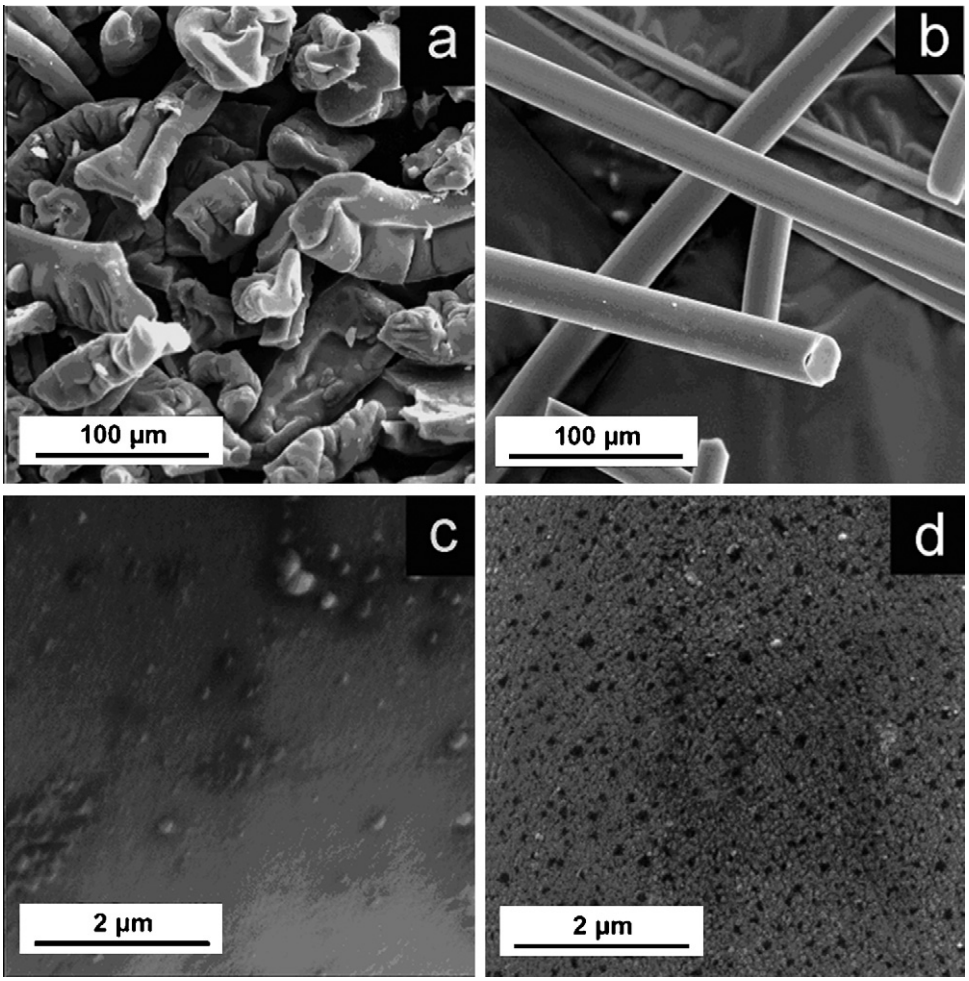

Fig. 7. SEM micrographs: overall images of (a) PTF-700 and (b) 0.15STF-700; surface morphologies of (c) PTF-700 and (d) 0.15STF-700.

3.5. BET specific surface area and pore structure

Textural parameters derived from the N_2 adsorption–desorption isotherm data were summarized in Table 1. It could be seen that the surface area and pore volume of Si-doped TiO_2 fibers treated in steam at 700 °C were obviously higher than that of the pure. This was mainly attributed to a proper concentration of silica going into the matrix, which would increase the defects in the TiO_2 fiber, restraining the samples from sintering and resulting in abundant mesopores [27,33]. Furthermore, the surface area and pore volume reached the maximum of 127.7 $m^2 g^{-1}$ and 0.25 $cm^3 g^{-1}$, respectively, when the Si/Ti molar ratio was 0.15. Large surface area and pore volume could enhance the rate of photocatalytic reaction because of high efficient adsorption of reactants and rapid diffusion of various products [8]. The high specific surface area and pore volume of the samples were expected to have a wider application in photocatalysis, selective adsorption, ultraviolet blockers, separation, sensing, and as functional filling materials in textile, paints, paper, and cosmetics.

The N_2 adsorption–desorption isotherms of the PTF-700 and 0.15STF-700 were presented in Fig. 8. The sample of 0.15STF-700 showed the type IV isotherms with type H1 hysteresis loops according to IUPAC classification, indicating the presence of mesopores (2–50 nm). However, PTF-700 sample exhibited typical type-V isotherms, which was considered to indicate nonporous in the range of mesopore corresponding to the SEM results. And the observed H3 hysteresis loops shifted to a high relative pressure $P/P_0 \approx 1$, suggesting the presence of large pores (>50 nm) [8]. Considering the morphology of the PTF-700 observed in Fig. 7a and c, the large pores might be attributed to the aggregation and breakage of the pure TiO_2 fibers. The inset of Fig. 8 showed the pore-size distributions of the samples by the DFT method. As for the 0.15STF-700, there was a narrow pore-size distribution ranging from 5.1

Table 1
Physical data of PTF-700 and Si-doped TiO_2 fibers.

Sample	BET surface area ($m^2 g^{-1}$)	Mean pore diameter (nm)	Peak diameter (nm)	Pore volume ($cm^3 g^{-1}$)	Shape
PTF-700	15.4	24.2	–[a]	0.07	Particles
0.05STF-700	89.0	10.4	8.2	0.22	Long fiber
0.10STF-700	115.3	8.6	7.0	0.23	Long fiber
0.15STF-700	127.7	8.3	6.1	0.25	Long fiber
0.20STF-700	114.9	7.2	5.5	0.19	Long fiber

[a] Not available.

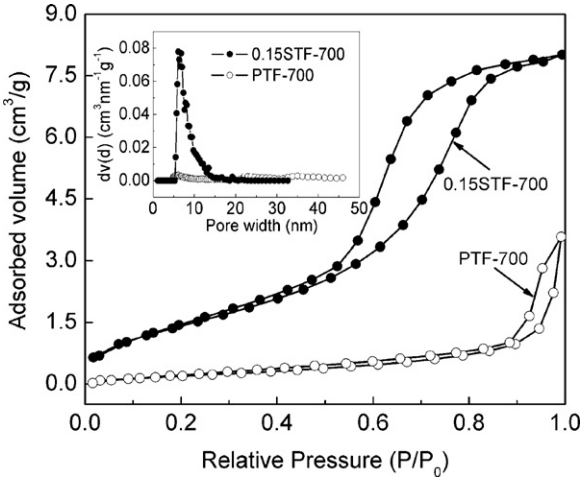

Fig. 8. N_2 adsorption–desorption isotherms and pore size distribution (inset) of PTF-700 and 0.15STF-700.

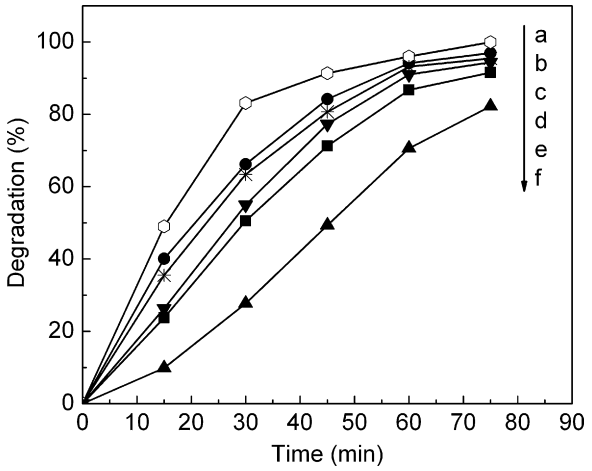

Fig. 10. Photocatalytic activity of 0.15STF heated at (a) 700 °C, (b) 500 °C, (c) 800 °C, (d) 900 °C, (e) 400 °C and (f) 600 °C.

to 9 nm with an average pore size of 8.3 nm, while there was no peak in mesopores region for the PTF-700. This confirmed the pore stability of the high temperature stable anatase as a result of silica doping under steaming condition. It was these mesopore structures that allowed rapid diffusion of products during UV illumination and enhance the rate of photocatalytic reaction, as seen subsequently.

3.6. UV–visible absorption spectra

The UV–visible spectra were measured to determine the optical absorption properties of the photocatalysts. Fig. 9 showed the UV–visible spectra of the TiO_2 fibers with different silica contents heated at 700 °C. Compared to pure titania sample, all Si-doped samples resulted in a substantial blue shift of the absorption edge, and absorption edges of PTF-700 and 0.15STF-700 were 441 and 429 nm, respectively. The band-gap energy of 0.15STF-700 calculated by the equation, E (eV) = 1239.95/λ (nm), was higher than others because of the blue shift that occurred due to doping. The increased band gap energy could be attributed to a combined effect of the quantum size and the interface interactions [27,33,42]. Possibly the increment in band gap would result in the reduction of electron-hole recombination rate generated during the illumination of TiO_2. It also can be seen in Fig. 9 that the absorption intensity of 0.15STF-700 was higher than that of other samples in the ultraviolet region. All these were beneficial for improving the oxidative ability and increasing the photocatalytic activity of the catalysts under ultraviolet irradiation.

3.7. Photocatalytic activity of TiO_2 fibers

3.7.1. Laboratory experiments

The photocatalytic activity of the catalysts was studied by using X-3B degradation experiments as explained in the experimental section. The dark adsorption study of the dye showed that there was some initial adsorption on the surface of the TiO_2 fibers for both Si-doped and undoped titania. In order to avoid any error due to the adsorption effects, the suspension was initially stirred for 30 min in the dark to establish the adsorption–desorption equilibrium between X-3B and the sample surface. As control experiments, photoactivity for X-3B in the dark in the presence of fibers and under UV irradiation in the absence of fibers was also evaluated. It was found that there was no degradation for the X-3B in the dark and in the presence of catalyst. Also no degradation was observed when the solution was irradiated under a UV lamp without the addition of catalyst.

Figs. 10 and 11 showed the photocatalytic activity of the 0.15STF heated at different temperatures and the samples with different silica contents heated at 700 °C, respectively. The heat treatment

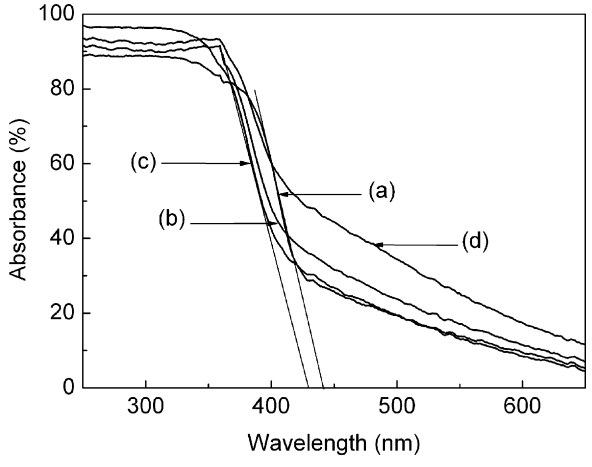

Fig. 9. UV–vis absorption spectra of (a) PTF-700, (b) 0.05STF-700, (c) 0.15STF-700 and (d) 0.20STF-700.

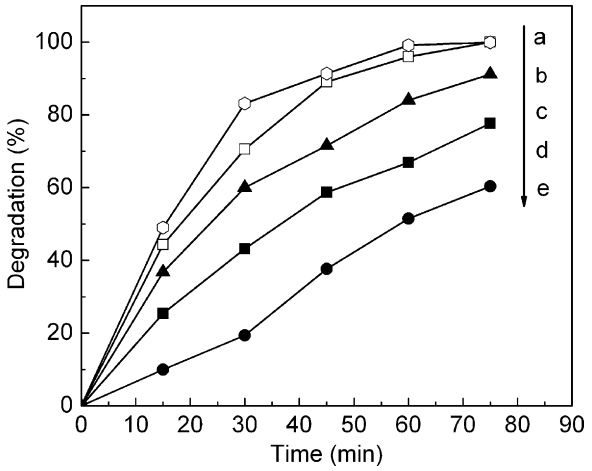

Fig. 11. Photocatalytic degradation profiles of X-3B over (a) 0.15STF-700, (b) PTF-700, (c) 0.10STF-700, (d) 0.20STF-700 and (e) 0.05STF-700.

temperatures and the silica contents were all important factors for photocatalytic activity of the catalyst. The 0.15STF sample, with heat treatment at 700 °C, had the highest decomposition rate of X-3B, which was about 99.6% for 75 min. This seemed to suggest that the decomposition of X-3B must be related to the structure of TiO_2. The silica doping would cause three main changes in the titania: i.e. anatase phase stability, increase in surface area and pore volume and the band gap changes. Anatase titania was reported to be more photocatalytically active than the rutile form because the adsorption affinity of organic dye molecule towards anatase phase was more compared to that toward rutile [43]. Moreover, anatase exhibited lower rates of electron-hole recombination in comparison with rutile due to its 10-fold greater rate of electron trapping [44]. Photocatalysis reactions mainly took place at the surface of the catalyst rather than in the bulk. So the specific surface area of the catalyst was also a key factor for the decomposition of X-3B. Silica doping could help to obtain large surface area as along with the porous structure. The sample of 0.15STF heated at 700 °C showed higher surface area and pore volume: 127.7 $m^2\,g^{-1}$ and 0.25 $cm^3\,g^{-1}$ (Table 1), where pure TiO_2 showed only 15.4 $m^2\,g^{-1}$ and 0.07 $cm^3\,g^{-1}$, respectively. This improvement in surface area by the addition of silica would help the adsorption of more dye molecules on the surface of the anatase titania, while high pore volume resulted in a rapid diffusion of various products during the photocatalytic reaction, leading to higher photocatalytic activity. Further more, the photogenerated intermediate oxidants such as hydroxyl and superoxide radicals generated could easily diffuse from the TiO_2 surface and react with dye molecules adsorbed on the adsorption active sites. Finally, the band gap changes in Si-doped titania also contributed towards the higher photocatalytic activity of doped titania in UV range. The band-gap energy of 0.15STF-700 was higher than that of undoped TiO2. This increment resulted in the reduction of electron–hole recombination rate generated during the illumination. In addition, the higher absorption intensity of 0.15STF-700 in the ultraviolet region could improve ultraviolet utilization rate, corresponding to better catalytic activity. It was strange that PTF-700 exhibited higher photoactivity than other samples except 0.15STF-700, although it had the smallest surface area. This may be because pure TiO_2 heated at 700 °C was the mixed form of the rutile and anatase structures, and the ratio of anatase and rutile was 68:32 (XRD result) close to that of the commercial photocatalyst Degussa P25 (70:30) known for its high photocatalystic activity. And, some authors had reported that TiO_2 consisting of anatase phase and rutile phase exhibited higher photoactivity used for some organic compounds decomposition than pure anatase [40,45].

The photocatalytic stability of 0.15STF-700 sample under ultraviolet irradiation was also evaluated by reusing experiments, and the result was shown in Fig. 12. The experimental parameters and processes were the same as above. After experiments, the filter screen with a pore size of 0.42 mm was used to separate TiO_2 fibers. Then, the fibers were washed using deionized water for 3 times and dried at 120 °C for 4 h. After 6 times reuse, the degradation rate of X-3B was still above 90%. The long Si-doped TiO_2 fibers exhibited potential value in industrial application because of its easy separation and high photocatalytic activity.

3.7.2. Solar experiments

The degradation profiles of X-3B using 0.15STF-700 as photocatalysts under solar irradiation were shown in Fig. 13. After 3 h irradiation, red had completely vanished, and the degradation rate of X-3B reached 94.7%. Meanwhile, the TOC decreased from 7.18 mg L^{-1} to 2.95 mg L^{-1} measured by total organic carbon analyzer, corresponding to the mineralization rate as high as 58.9%. The high solar photocatalytic activities and stability made the catalysts promising materials for water treatment, on account of easy recycling and reusing.

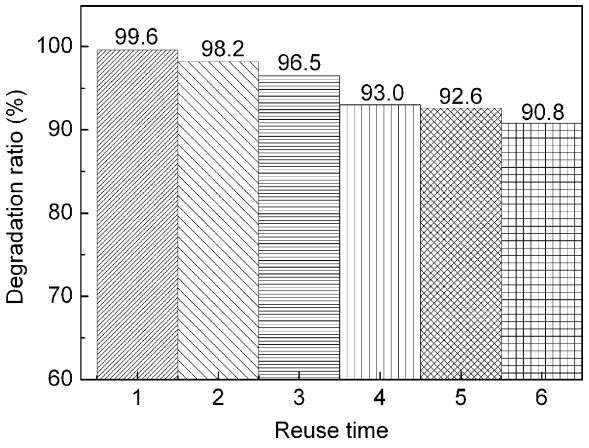

Fig. 12. Degradation rate of X-3B after 75 min of UV irradiation for different reusing times.

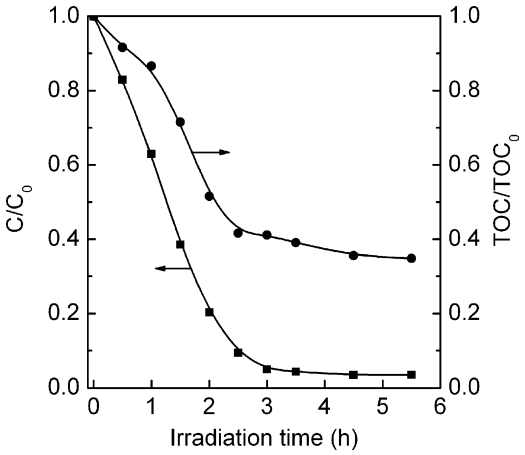

Fig. 13. Photocatalytic degradation profiles of X-3B using 0.15STF-700 under solar irradiation.

4. Conclusions

Long Si-doped mesoporous TiO_2 fibers, which were consisted of nanoparticles and abundant mesopores, were successfully prepared using TBOT and TEOS as precursors by a facile method of the combination of sol–gel process and centrifugal spinning. We could control the crystal phase, surface area and porous structure by varying the contents of silica and the heat treatment temperatures in steam. Compared to the pure titania, the addition of silica was a crucial factor for obtaining long fibers because of the formation of Ti–O–Si networks. Moreover, the proper addition of silica into titania could enhance the thermal stability and crystal stability, for example, suppressed the phase transformation of titania from anatase to rutile, prevented the growth of titania grains, and increased surface area. The study showed that the sample of 0.15STF gave fully anatase phase at 900 °C whereas the pure titania was partially converted to rutile at 700 °C. Again, the 0.15STF-700 retained the maximal surface area and pore volume, 127.7 $m^2\,g^{-1}$ and 0.25 $cm^3\,g^{-1}$, respectively. The photocatalytic properties of the samples were studied by the degradation of reactive brilliant red X-3B in aqueous solution. In this case, the silica contents and the heat treatment temperatures of TiO_2 fibers largely influenced their photocatalytic activity. The results indicated that the most opti-

mal material for high photocatalytic activity was the sample of 0.15STF heated at 700 °C in stream atmosphere, and it displayed good stability evaluated by reusing experiments. Furthermore, the 0.15STF-700 could effectively photodecompose and mineralize X-3B under solar irradiation, and could be easily separated and recycled from solutions because of the advantages of the unique fiber morphology, which made the photocatalyst promising functional materials for removal and degradation of organic pollutants in water.

Acknowledgements

The authors acknowledge the financial support of the State 863 Projects (China No. 2003AA601060) and the Youth Foundation of Shandong University (China No. 11440053187025). We thank Prof. P. D. Holt for manuscript preparation.

References

[1] A. Corma, From microporous to mesoporous molecular sieve materials and their use in catalysis, Chem. Rev. 97 (1997) 2373–2419.
[2] A. Fujishima, T.N. Rao, D.A. Tryk, Titanium dioxide photocatalysis, J. Photochem. Photobiol. C 1 (2000) 1–21.
[3] X.H. Qi, Z.H. Wang, Y.Y. Zhuang, Y. Yu, J.L. Li, Study on the photocatalysis performance and degradation kinetics of X-3B over modified titanium dioxide, J. Hazard. Mater. B 118 (2005) 219–225.
[4] V. Augugliaro, V. Loddo, G. Marci, L. Palmisano, M.J. Lopez-Munoz, Photocatalytic oxidation of cyanides in aqueous titanium dioxide suspensions, J. Catal. 166 (1997) 272–283.
[5] F. Sayilkan, S. Erdemoglu, M. Asilturk, M. Akarsu, S. Sener, H. Sayilkan, M. Erdemoglu, E. Arpac, Photocatalytic performance of pure anatase nanocrystallite TiO_2 synthesized under low temperature hydrothermal conditions, Mater. Res. Bull. 41 (2006) 2276–2285.
[6] X.H. Xia, Y. Liang, Z. Wang, J. Fan, Y.S. Luo, Z.J. Jia, Synthesis and photocatalytic properties of TiO_2 nanostructures, Mater. Res. Bull. 43 (2008) 2187–2195.
[7] H.M. Zhang, X. Quan, S. Chen, H.M. Zhao, Fabrication and characterization of silica/titania nanotubes composite membrane with photocatalytic capability, Environ. Sci. Technol. 40 (2006) 6104–6109.
[8] J.G. Yu, H.G. Yu, B. Cheng, X.J. Zhao, Q.J. Zhang, Preparation and photocatalytic activity of mesoporous anatase TiO_2 nanofibers by a hydrothermal method, J. Photochem. Photobiol. A 182 (2006) 121–127.
[9] M. Iida, T. Sasaki, M. Watanabe, Titanium dioxide hollow microspheres with an extremely thin shell, Chem. Mater. 10 (1998) 3780–3782.
[10] L.Z. Wang, T. Sasaki, Y. Ebina, K. Kurashima, M. Watanabe, Fabrication of controllable ultrathin hollow shells by layer-by-layer assembly of exfoliated titania nanosheets on polymer templates, Chem. Mater. 14 (2002) 4827–4832.
[11] S. Horikoshi, A. Saitou, H. Hidaka, N. Serpone, Environmental remediation by an integrated microwave/UV illumination method. V. Thermal and nonthermal effects of microwave radiation on the photocatalyst and on the photodegradation of rhodamine-B under UV/vis radiation, Environ. Sci. Technol. 37 (2003) 5813–5822.
[12] H. Al-Ekabi, N. Serpone, Kinetics studies in heterogeneous photocatalysis. I. Photocatalytic degradation of chlorinated phenols in aerated aqueous solutions over titania supported on a glass matrix, J. Phys. Chem. 92 (1988) 5726–5731.
[13] S.R. Mukai, H. Nishihara, S. Shichi, H. Tamon, Preparation of porous TiO_2 cryogel fibers through unidirectional freezing of hydrogel followed by freeze-drying, Chem. Mater. 16 (2004) 4987–4991.
[14] Q. Chen, J.W. Cui, P. Song, W. Chen, M.F. Zhou, Y.J. Zhang, Study on the gelation and heat-treatment of TiO_2 fibers prepared by the hydrolysis of $Ti(OC_4H_9)_4$, J. Inorg. Mater. 6 (1991) 249–255.
[15] S. Yin, Y. Fujishiro, J.H. Wu, M. Aki, T. Sato, Synthesis and photocatalytic properties of fibrous titania by solvothermal reactions, J. Mater. Process. Technol. 137 (2003) 45–48.
[16] N.Z. Bao, X. Feng, Z.H. Yang, L.M. Shen, X.H. Lu, Highly efficient liquid-phase photooxidation of an azo dye methyl orange over novel nanostructured porous titanate-based fiber of self-supported radially aligned $H_2Ti_8O_{17}\cdot 1.5H_2O$ nanorods, Environ. Sci. Technol. 38 (2004) 2729–2736.
[17] N.Z. Bao, L.M. Shen, K. Yanagisawa, Textural and catalytic properties of combinational micro-mesoporous octatitanate fibers prepared by solvothermal soft chemical process, J. Phys. Chem. B 108 (2004) 16739–16745.
[18] M. He, X.H. Lu, X. Feng, L. Yu, Z.H. Yang, A simple approach to mesoporous fibrous titania frompotassium dititanate, Commun 17 (2004) 2202–2203.
[19] Z.H. Yang, N.Z. Bao, C. Liu, X. Feng, J.W. Xie, X.Y. Ji, X.H. Lu, Preparation of titanium dioxide fibers and their photocatalysis reactivity, Chem. J. Chin. Univ. 23 (2002) 1371–1374.
[20] S. Madhugiri, B. Sun, P.G. Smirniotis, J.P. Ferraris, K.J. Balkus Jr., Electrospun mesoporous titanium dioxide fibers, Micropor. Mesopor. Mater. 69 (2004) 77–83.
[21] S.H. Zhan, D.R. Chen, X.L. Jiao, Long TiO_2 hollow fibers with mesoporous walls: sol–gel combined electrospun fabrication and photocatalytic properties, J. Phys. Chem. B 110 (2006) 11199–11204.
[22] T. Ishikawa, H. Yamaoka, Y. Harada, T. Fujii, T. Nagasawa, A general process for in situ formation of functional surface layers on ceramics, Nature 416 (2002) 64–67.
[23] T. Matsunaga, H. Yamaoka, S.I. Ohtani, Y. Harada, T. Fujii, T. Ishikawa, High photocatalytic activity of palladium-deposited mesoporous TiO_2/SiO_2 fibers, Appl. Catal. A: Gen. 351 (2008) 231–238.
[24] N. Bao, Z.H. Ma, F. Zhang, J. Sun, C.L. Zhang, CN: ZL200620081025.X.
[25] R.A. Spurr, H. Myers, Quantitative analysis of anatase-rutile mixtures with an X-ray diffractometer, Anal. Chem. 29 (1957) 760–762.
[26] N. Bao, J.S. Wang, C.R. Deng, Y.J. Chen, Immobilized photocatalytic oxidation offuraltadone in aqueous solution, Chin. Environ. Sci. 18 (1998) 458–462.
[27] P. Periyat, K.V. Baiju, P. Mukundan, P.K. Pillai, K.G.K. Warrier, High temperature stable mesoporous anatase TiO_2 photocatalyst achieved by silica addition, Appl. Catal. A: Gen. 349 (2008) 13–19.
[28] M. Yoshinaka, K. Hirota, O. Yamaguchi, Formation and sintering of TiO_2 (anatase) solid solution in the system TiO_2–SiO_2, J. Am. Ceram. Soc. 80 (1997) 2749–2753.
[29] P. Cheng, M.P. Zheng, Y.P. Jin, Q. Huang, M.Y. Gu, Preparation and characterization of silica-doped titania photocatalyst through sol–gel method, Mater. Lett. 57 (2003) 2989–2994.
[30] H. Shibata, T. Ohkubo, H. Kohno, P. Rangsunvigit, H. Sakai, M. Abe, Preparation and photocatalytic activity of titania particulate film with mesostructured silica as binder, J. Photochem. Photobiol. A 181 (2006) 357–362.
[31] D.C.M. Dutoit, M. Schneider, A. Baiker, Titania-silica mixed oxides. I. Influence of sol–gel and drying conditions on structural properties, J. Catal. 153 (1995) 165–176.
[32] Z.F. Liu, J. Tabora, R.J. Davis, Relationships between microstructure and surface acidity of Ti–Si mixed oxide catalysts, J. Catal. 149 (1994) 117–126.
[33] X.T. Gao, I.E. Wachs, Titania-silica as catalysts: molecular structural characteristics and physico-chemical properties, Catal. Today 51 (1999) 233–254.
[34] H. Kochkar, F. Figueras, Synthesis of hydrophobic TiO_2–SiO_2 mixed oxides for the epoxidation of cyclohexene, J. Catal. 171 (1997) 420–430.
[35] X.Z. Fu, L.A. Clark, Q. Yang, M.A. Anderson, Enhanced photocatalytic performance of titania-based binary metal oxides: TiO_2/SiO_2 and TiO_2/ZrO_2, Environ. Sci. Technol. 30 (1996) 647–653.
[36] R. Castillo, B. Koch, P. Ruiz, B. Delmon, Influence of the amount of titania on the texture and structure of titania supported on silica, J. Catal. 161 (1996) 524–529.
[37] S. Music, M. Gotic, M. Ivanda, S. Popovic, A. Turkovic, R. Trojko, A. Sekulic, K. Furic, Chemical and micro structural properties of TiO_2 synthesized by sol–gel procedure, Mater. Sci. Eng. B 47 (1997) 33–40.
[38] M. Schraml-Marth, K.L. Walther, A. Wokaum, B.E. Handy, A. Baiker, Porous silica gels and TiO_2/SiO_2 mixed oxides prepared via the sol–gel process: characterization by spectroscopic techniques, J. Non Cryst. Solids 143 (1992) 93–111.
[39] J. Kiwi, M. Grätzel, Characterization of $(SiW_{12}O_{40})^{4-}/TiO_2$ suspensions and their activity in the evolution of hydrogen from water, J. Phys. Chem. 91 (1987) 6673–6677.
[40] R.R. Bacsa, J. Kiwi, Effect of rutile phase on the photocatalytic properties of nanocrystalline titania during the degradation of p-coumaric acid, Appl. Catal. B: Environ. 16 (1998) 19–29.
[41] A.L. Linsebigler, G.Q. Lu, J.T. Yates, Photocatalysis on TiO_2 surfaces: principles, mechanisms, and selected results, Chem. Rev. 95 (1995) 735–758.
[42] M. Anpo, T. Shima, S. Kodama, Y. Kubokawa, Photocatalytic hydrogenation of CH_3CCH with H_2O on small-particle TiO_2: size quantization effects and reaction intermediates, J. Phys. Chem. 91 (1987) 4305–4310.
[43] D.C. Hurum, A.G. Agrios, K.A. Gray, Explaining the enhanced photocatalytic activity of Degussa P25 mixed-phase TiO_2 using EPR, J. Phys. Chem. B 107 (2003) 4545–4549.
[44] G. Riegel, J.R. Bolton, Photocatalytic efficiency variability in TiO_2 particles, J. Phys. Chem. 99 (1995) 4215–4224.
[45] Y.J. Li, X.D. Li, J.W. Li, J. Yin, TiO_2-coated active carbon composites with increased photocatalytic activity prepared by a properly controlled sol–gel method, Mater. Lett. 59 (2005) 2659–2663.